water

MDPI

Article

Effects of Patch Density and Incoming Sediment on Flow Characteristics and Bed Morphology

Dan Wang [1], Feng Li [2] and Kejun Yang [1,*]

[1] State Key Laboratory of Hydraulics and Mountain River Engineering, Sichuan University, Chengdu 610065, China; wangdan_cherry@126.com
[2] Chongqing Xike Consultation for Water Transport Co., Ltd., Chongqing 400042, China; sculifeng@163.com
* Correspondence: yangkejun@scu.edu.cn

Abstract: This study focuses on the effects of vegetation patch density, bed condition, and incoming sediment on flow structure and bed morphology within and around a patch. The variation in upstream adjustment velocity is not well defined for low-density vegetation patches but decreases with increasing patch density in high-density patches. The length of the upstream adjustment region is greater for high-density vegetation. Incoming sediment causes a reduction in both the steady wake velocity and the length of the steady wake at a low density. The length of the recovery region increases with density when vegetation is sparse, but remains constant in a dense patch. Additionally, the length of the recovery region decreases due to incoming sediment. Turbulent kinetic energy is not affected by the bedform and incoming sediment when reaching its first peak. However, the second maximum of the turbulent kinetic energy increases when the bed is movable. The evolution of bed morphology is closely related to the flow structure and the growth of the von Karman vortex street. Both the rising length and the adjusted length decrease with increasing patch density, while the incoming sediment causes an increase in the adjusted length. Behind the patch wake, the first minimum elevation, maximum elevation, and second minimum elevation decrease as the patch density increases. These values, in turn, increase with the sediment supply upstream of the flume.

Keywords: vegetation patch; density; velocity; turbulent kinetic energy; bed morphology

Citation: Wang, D.; Li, F.; Yang, K. Effects of Patch Density and Incoming Sediment on Flow Characteristics and Bed Morphology. *Water* **2023**, *15*, 3247. https://doi.org/10.3390/w15183247

Academic Editor: Giuseppe Oliveto

Received: 22 June 2023
Revised: 26 August 2023
Accepted: 29 August 2023
Published: 12 September 2023

1. Introduction

Aquatic plants are widespread in natural rivers, man-made open channels, and coastal waters and can significantly affect water flow structure. In particular, the vegetation not only has an impact on the distribution of velocity but also has a major effect on the structure and diffusion of turbulence. This is mainly reflected in the Reynolds stress of the flow, the secondary flow, and the horizontal vortex at the water-plant interface [1,2]. The interaction between river flow and aquatic vegetation generates specific and complex flow patterns, partly due to interactions with various types of aquatic plants. For example, both emergent vegetation (such as phyllostachys heteroclada) and submergent vegetation (such as algae) are common in natural rivers. Depending on the type, vegetation can grow on floodplains, at the bottom of riverbeds, or in the water itself. The interaction between vegetation and water depends not only on the water level, flow velocity, and bed morphology but also on various characteristics of vegetation patches, such as species, size, density, stiffness, and community structure [3–5]. Aquatic vegetation often covers parts of the channel bed, changing the ecosystem of a river from a continuous space to a partially continuous space [6]. These conditions and characteristics create intricate contact interfaces between the channels, water flow, and vegetation, which in turn further complicate the flow structure and energy transfer.

The interactions between aquatic vegetation and river flow can have both positive and negative impacts on a river's ecosystem. Many aquatic plants can adsorb and even

degrade several harmful substances in water, such as heavy metals, nitrogen, phosphorus, and other toxic and hazardous compounds. Therefore, the presence of these plants can purify and improve river water quality and the environment [7]. Aquatic vegetation in rivers reduces the flow velocity around the vegetated area, thereby reducing the shear stress on the river bed and protecting the riverbed from erosion and scour [8,9]. A reduction in flow velocity can cause the deposition of suspended sediment, which increases water transparency. In terms of negative impacts, the presence of aquatic vegetation causes increased flow resistance, leading to higher water levels and thus an increased risk of flooding [10,11]. Moreover, an increase in the flow resistance of aquatic plants alters the flow structure, converting some flow energy into turbulent kinetic energy (TKE) in the vicinity of the vegetation. This affects the kinetic energy of the flow and the characteristics of the flow energy being transferred and dissipated [12–14]. Therefore, it is important to determine the velocity distribution and the discharge capacity of a water channel.

Sediment is another key indicator that is impacted by a river's ecosystem. Sediment transport frequently occurs in natural channels and affects flow structure as a result of the interaction between the flow, vegetation, and sediment. The root systems of the vegetation enhance the soil's stability, thereby increasing the critical shear stress required for the incipient motion of sediment. Consequently, the erosion and deposition statuses of the riverbed are weakened, and soil erosion is reduced [15]. Plants can promote the stability of the riverbed and decrease bank erosion [16]. Sediment transport has been studied for many years due to its practical importance, and research has mainly focused on the investigation of the laws governing sediment movement, especially for sediment-laden flows with low to medium concentrations.

In natural rivers and coastal ecosystems, vegetation tends to grow into communities that entail biological competition and cover at least part of the channel. For this reason, these types of vegetation are known as "vegetation patches" and can affect flow structure and bed morphology in various ways, different from the effects created by individual plants. Temmerman et al. analyzed the variation in the growth of an aquatic vegetation community [17]. They found that the initial growth pattern was similar to a cylinder before it developed into other patterns. The characteristics of the patch, such as plant type, density, and arrangement, can significantly alter the flow structure, and these factors can be used to predict and calculate flow velocity [18,19]. Currently, most research conducted on vegetation patches concentrates on the impact of individual vegetation patches on flow hydrodynamic characteristics and sedimentation within the patch. A study by Rominger and Nepf showed that the flow adjustment region was associated with canopy flow blockage, and this is a function of the width and porosity of obstructions [14]. The internal adjustment length was determined using the array's frontal area per unit volume for a low flow blockage, while the array width was used to determine the interior adjustment length within the porous obstruction for a high flow blockage. Follett and Nepf described the sediment patterns formed in a sand bed around circular patches of rigid vertical cylinders [20]. It was reported that scour was positively correlated with its TKE. Chen et al. studied the mean and turbulent flow structures in the wake of a circular array of cylinders and proposed a method to estimate the wake length behind sparse and dense patches [21]. Ortiz et al. investigated how the spatial distribution of flow is connected to the spatial distribution of suspended sediment deposition [22]. Recently, some studies have shown that the turbulence generated by vegetation can affect sediment transport and enhance sediment suspension [23–26]. Therefore, water flow in the presence of vegetation patches has its own characteristics, and issues related to water flow within vegetation communities need to be investigated to solve practical engineering problems.

Previous literature reviews highlighted some features of the effects of vegetation patches on flow structure and sediment deposition, but generally, previous research primarily focused on alterations in velocity distribution and sediment subsidence near the vegetation patch. Furthermore, to the best of our knowledge, the effects of sediment supply on flow structure and bed morphodynamics in vegetation flow remain unexplored. Herein,

systematic laboratory experiments were conducted to investigate the characteristics of the velocity distribution, TKE distribution, and bed morphodynamics in a flume with a vegetation patch and sediment supply. This study aims to analyze how patch density and feeding sediment affect bed morphology when combined with velocity and TKE distribution. Meanwhile, another purpose is to explore the underlying mechanisms of these effects and determine whether sediment near vegetation patches is deposited as feeding sediment. This study analyzes the effects of patch density and sand supply in channels on flow, energy, and the resulting channel morphology. This research is relevant to river restoration projects and may provide insights into restoration strategies and management plans for channels. The primary concept of exploring the effects of incoming sediment on vegetation patches could prove groundbreaking and will certainly appeal to the ecohydraulics research community. This research will not only provide powerful insights for improving the prediction of sediment transport in natural river environments but also provide a scientific basis for ecological river restoration and natural channel construction.

2. Experimental Procedures and Measurement Methods

2.1. Experimental Arrangement

Laboratory experiments were conducted using a straight Plexiglas flume (16 m length $\times$ 0.3 m width $\times$ 0.4 m height) with a 1.62 m long test section at the State Key Hydraulics Laboratory of Sichuan University. A valve was set upstream of the flume to control the flow rate, and the water entered a reservoir via the valve. Then, the water flowed into a quiescent tank through a triangular weir when the reservoir was full, and finally flowed into the flume via an energy dissipation grid. The bottom of the flume was covered with perforated PVC. A gate was installed at the end of the flume to control the water surface. A funnel with a filter screen controlled by a valve was placed upstream of the plate gate to collect sand.

The flow quantity of 0.018 m^3/s and the cross-sectional area of 375 $\pm$ 6 cm^2 were kept constant in this study. As a result, the cross-sectional mean velocity (U_0) of the upstream flow, calculated from the cross-sectional area, was also kept constant at 48 $\pm$ 0.3 cm/s. The slope of the flume was measured with a spirit level and maintained at 1‰. To ensure a uniform flow, the water depth was measured at 13 cross-sections every 0.8 m. The water depth was measured every 30 min with a water-level sensor until the depths at all 13 cross-sections were approximately the same. An electrically powered delivery platform located at the entrance of the flume was used to continuously feed sand into the flume at a set rate. The sand was spread evenly on the platform, which was then rotated by a motor, causing it to fall into the flume. A certain amount of sand (1.2 kg) was evenly added to the flume every 10 min.

Bamboo stems were used to model the emergent vegetation patch and were placed in a PVC plate with uniform holes. The stem diameter was 0.4 cm. The circular model vegetation patch with a prescribed density was placed at the center of the flume (see Figure 1a). The diameter of the model patch (D) in this study was designed to be 6 cm, blocking 20% of the channel width (30 cm). The patch density (a) was varied and can be estimated using the following equation:

$$a = nd \tag{1}$$

where d (cm) is the diameter of a single plant and n (cm^{-2}) is the number of plants in a unit area of vegetation, which, in turn, is the ratio of the number of all the plants and the vegetation area. The vegetation density varied from 0.2 cm^{-1} to 0.7 cm^{-1} in the rigid bed, and this range of values encompasses the densities in many laboratory studies or observations conducted in real aquatic vegetation systems. For example, Furukawa et al. observed that the density of mangroves in the field can be as high as 1.6 cm^{-1} [27]. The stream-wise velocity behind the vegetation patch revealed that there was a critical patch density of a = 0.4 cm^{-1}, which is evidenced by different trends of the velocity distribution in the wake of the model patch [28]. Therefore, vegetation with a density of less than

0.4 cm^{-1} can be defined as sparse vegetation; otherwise, it can be defined as dense vegetation. Moreover, the longitudinal distribution shape of the depth-averaged velocity was only minimally affected by the bed form [29]. In this study, only two densities were set for the conditions of a movable bed and feeding sediment. The density for a sparse vegetation patch was 0.25 cm^{-1}, and the density for a dense vegetation patch was 0.5 cm^{-1}. The experimental parameters and conditions are given in Table 1.

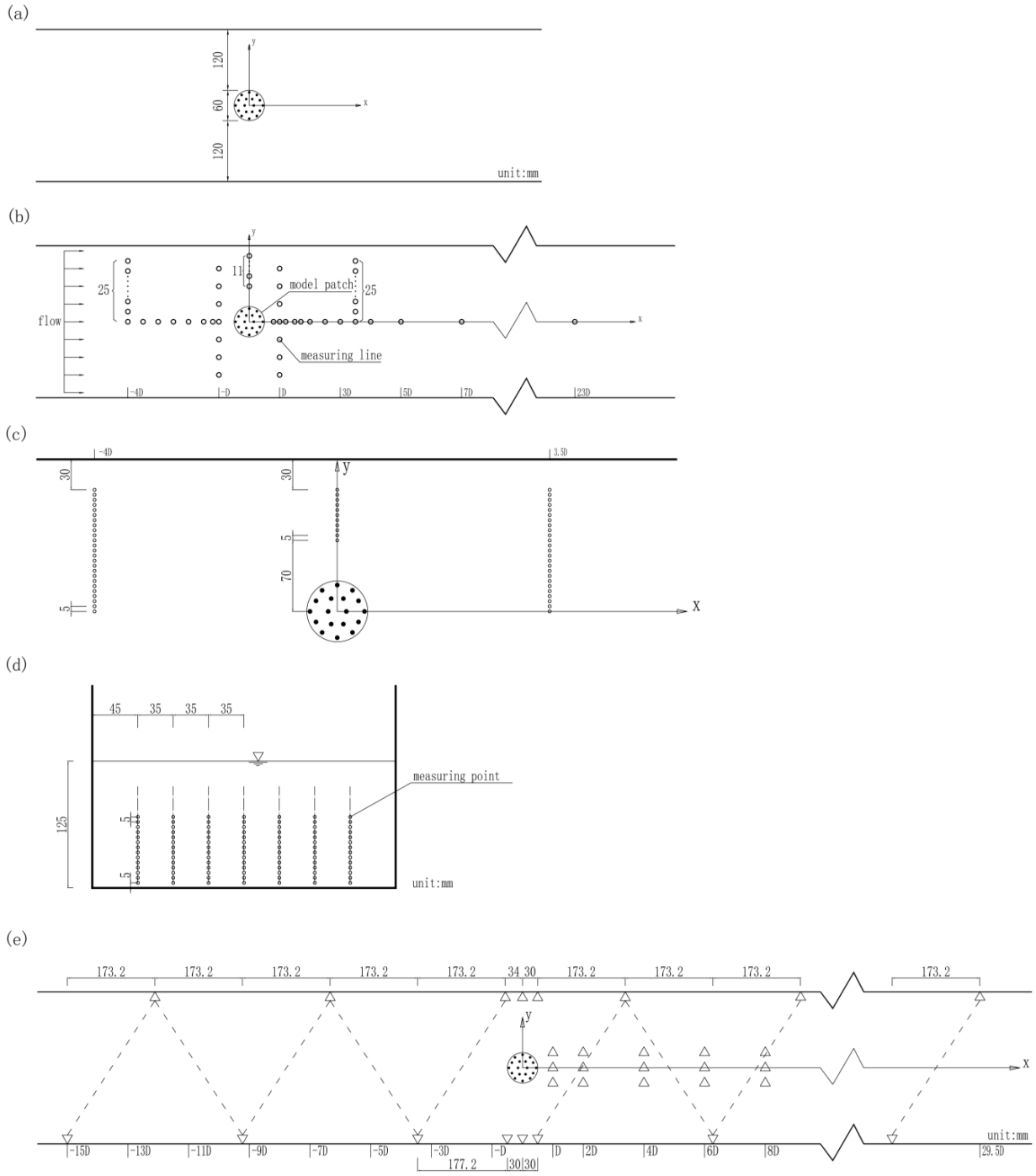

Figure 1. Layout of the model patch, measuring cross-sections, vertical lines, and points. (**a**) Location of the model patch. (**b**) Layout of measuring cross-sections and lines. (**c**) Enlarged view of measuring lines in sections $x/D = -4$, 0, 3.5. There are many measuring lines in these sections where the distance between the neighboring lines is too small; therefore, the details cannot be shown clearly in (**b**). (**d**) Measuring points in each line. (**e**) Layout of measuring points of the bed elevation.

Table 1. Test conditions.

Condition.	D (cm)	a (cm^{-1})	Ψ (%)	Bed Form
Anr0	Non-vegetated		0	rigid
Anr1	6	0.2	6	rigid
Anr2	6	0.25	8	rigid
Anr3	6	0.3	10	rigid
Anr4	6	0.4	13	rigid
Anr5	6	0.5	16	rigid
Anr6	6	0.6	19	rigid
Anr7	6	0.7	22	rigid
Anm0	Non-vegetated		0	movable
Anm1	6	0.25	8	movable
Anm2	6	0.5	16	movable
Anf0	Non-vegetated		0	feeding sediment
Anf1	6	0.25	8	feeding sediment
Anf2	6	0.5	16	feeding sediment

In the case of a movable bed, the bed was paved with uniform sediment (0.08 m thick and 12 m long), and the original bed elevation was about 0.6 m. The diameter of the sediment was estimated to be 1–2 mm based on the Sharmov formula and a preliminary test.

$$\frac{U_c}{\sqrt{gD_s}} = 1.47\left(\frac{H}{D_s}\right)^{\frac{1}{6}} \quad (2)$$

where U_c is the incipient velocity of sediment moving, g is the gravitational acceleration, and D_s is the diameter of the sediment. In the movable and feeding sediment bed cases, the valve was open when the velocity was measured and closed when the experiments were completed. The bed elevation can be conveniently and efficiently measured once all the water on the sand surface has flowed away. Specifically, the bed morphology was not isolated during the drainage process. The arrangement of the measuring points was initiated 0.9 m ($x/D = -15$) upstream of the model patch and terminated 1.8 m ($x/D = 29.5$) downstream of the vegetation patch. These points were distributed along both sides of the flume banks in an approximately continuous equilateral triangle, with adjacent points on each side of the bank 34.64 cm apart (see Figure 1e). In particular, slightly denser sampling points were added near the model patch ($-0.5D$–$8D$) because the flow through the vegetation patch affected the sediment deposition in the vicinity [20].

The longitudinal coordinate was defined as x in the direction of flow, called the streamwise direction below, with the center of the model patch at $x = 0$ (see Figure 1). The lateral coordinate is defined by y, where $y = 0$ is at the centerline of the flume. The vertical coordinate is z and $z = 0$ represents the bed. The flow velocity was measured upstream and downstream of the patch using a three-dimensional Sentek Vectrino Acoustic Doppler Velocimeter (ADV). Sampling with the ADV was taken from the bottom surface to mid-depth. At each sampling point, the three velocity components (u, v, w) were recorded at 50 Hz for 30–90 s. Velocities were measured at eight cross-sections upstream and twenty cross-sections downstream of the model patch, covering from $-4D$ to $23D$ (see Figure 1b). It was found that the flow near the wake of the model patch was drastically altered in the preparatory test before the formal measurement test. Therefore, more measurement cross-sections were arranged near the model patch, and the intervals were $0.2D$–$0.5D$ from the wake edge of the vegetation patch to Section $4D$. Then, the intervals between the adjacent sections behind $x/D = 5$ were equal, and of which were $2D$. Due to the flow obstruction caused by the model patch, there were 11 lines in the section $x/D = 0$. The position of these lines started 7 cm from the center of the patch towards the left bank. The distance between two neighboring test lines was 5 mm (see Figure 1c). In particular, there were seven vertical lines in the sections $x/D = \pm 1$, with a distance of 3.5 cm between the neighboring lines. These lines can be used to compare the distribution of velocities near

the upstream and downstream regions of the vegetation patch. Velocities in other sections were only measured along the centerline. The test points for each test line were distributed uniformly with a distance of 5 mm between each point (Figure 1d). Due to the constraints of the measuring equipment, measurements can only be carried out from a minimum height of 5 mm above the bed surface.

2.2. Experimental Methods

The depth-averaged velocity (U_d) may be calculated by integrating the velocities that are measured vertically throughout the depth of the water,

$$U_d = \frac{1}{H}\int_0^h u\, dz \tag{3}$$

where H is the water depth and u is the instantaneous streamwise velocity. A flow depth of $H = 12.5 \pm 0.2$ cm was set in this study. The turbulent kinetic energy (TKE) reflects the variation in the instantaneous three-dimensional flow velocity and can be calculated as follows:

$$TKE = \frac{1}{2}(\overline{u'^2} + \overline{v'^2} + \overline{w'^2}) \tag{4}$$

where u', v' and w' are the longitudinal, lateral, and vertical fluctuating velocities, respectively. The overbar represents the time-averaged values. Matlab was used to calculate the TKE based on processing the raw measurement data of the centerline, where the z-location was $0.5H$ in each section.

The volume fraction, φ, denotes the dimensionless density of the vegetation patch and is defined as $\varphi = 1 - e$, where e is the void ratio of the patch. It can be calculated using the following equation:

$$e = \frac{V_0 - V_1}{V_0} \times 100\% \tag{5}$$

where V_0 is the volume of the vegetation patch per unit volume, and $V_0 = \frac{\pi D^2}{4}$. Additionally, V_1 is the volume of a cylinder per unit volume, and $V_1 = \frac{N\pi d^2}{4}$, in which N is the number of cylinders. In this experiment, φ varies from 6% to 22% for the rigid bed case (Table 1). There are only two groups in the case of movable beds and feeding sediment, defined as sparse and dense patches, respectively, with $\varphi = 8\%$ and $\varphi = 16\%$.

3. Results

3.1. Leading Edge

The velocity distribution of the flow with a vegetation patch differs from that of traditional open channel flow. Water flowing through a porous medium forms a wake structure. Similarly, the fluid passing through the vegetation patch also forms a wake pattern. Far upstream, the presence of a vegetation patch has a negligible impact on the flow structure, except at the leading edge of the patch. Some significant features of the flow reveal that the velocity slightly decelerates for a short distance before the vegetation patch in all cases. This depleted region is defined as the upstream adjustment region, and its length is denoted as L_0 (Figure 2a). The velocity at the front end of the patch, denoted by U_a at the leading edge of the patch, is clearly less than that far upstream (Figure 2a).

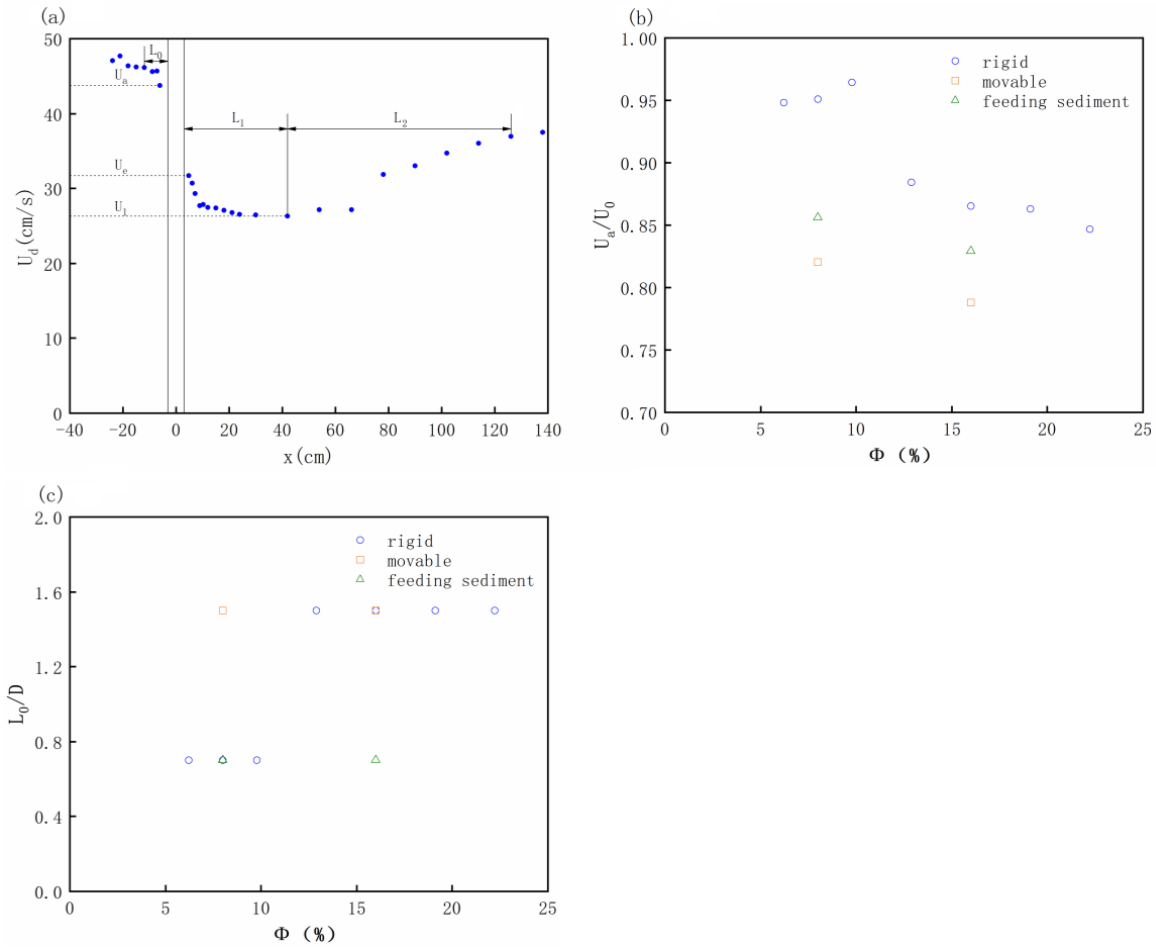

Figure 2. (**a**) The schematic of all the characteristic lengths and velocities. (**b**) The dimensionless distribution of the upstream adjustment velocity (U_a/U_0). (**c**) The dimensionless distribution of the upstream adjustment length (L_0/D).

In a rigid bed, the upstream adjustment velocity U_a corresponding to each density varies in sparse and dense cases. The dimensionless distribution illustrates that U_a/U_0 stays almost constant when $\varphi < 10\%$, i.e., $U_a \approx 0.95U_0$. However, for $\varphi > 10\%$, the dimensionless ratio decreases fractionally as the volume fraction increases, and all the ratios are less than 0.9. Additionally, in both cases of a movable bed and feeding sediment, the upstream adjustment velocity for the sparse patch is greater than for the dense one (see Figure 2b). However, given that there are an insufficient number of density gradient experiments, it is hard to determine whether the upstream adjustment velocity changes with patch density in these cases. When comparing different bed conditions, it is clear that the ratio of U_a/U_0 is disparate, but the ratio for the low-density case is greater than that for the high-density case. The ratio for the rigid bed is maximum but is minimum for the movable bed in both the low-density and high-density cases (see Figure 2b). At the leading edge of the vegetation patch, the flow resistance changes in steps as a result of the increased vegetation drag; meanwhile, the current starts to reduce the velocity in response to the addition of pressure. The pressure gradient can cause a lateral diversion of fluid in the upstream area of the vegetation patch, i.e., the flow adjustment region approaching the leading edge of the patch. When the bed is rigid, only the interaction between the flow and the vegetation can affect velocity. With an increase in the density of the vegetation patch, the water-blocking area is enlarged and the flow resistance improves, which results in a decline in velocity at the leading edge of the patch. In contrast, the water blocking capacity does not greatly vary with density for the sparse vegetation patch, which explains why the velocity of upstream adjustment remains constant for the low-density patch. When

the bed is movable, the sediment interacts with the water and the vegetation, resulting in sediment transport, and this process consumes energy so that the velocity near the patch drops. Additionally, enhanced bottom roughness by the sediment results in stronger bed shear stress, which further reduces the velocity. In the feeding sediment case, sediment is supplied upstream of the flume, and sediment on the bed accumulates. Moreover, given the constant discharge far upstream, the water depth decreases, and the velocity around the leading edge of the patch increases.

In addition, there are some differences in the variation of the upstream adjustment length for each case (Figure 2c). The dimensionless length of the high-density vegetation patch is about 1.5, which is greater than that of the low-density patch in the case of a rigid bed. This value remains relatively constant whether the patch is sparse or dense, while, for movable bed and feeding sediment cases, the dimensionless upstream adjustment length is the same whether the patch is sparse or dense. The ratio for the movable bed case is greater than that for the feeding sediment case, with values of 0.7 and 1.5, respectively. The interactions between water and patches are less complex than those between water, vegetation, and sediment. As indicated in Figure 2c, the upstream adjustment length only depends on the patch density in the case of a rigid bed. As sand is supplied upstream of the flume, sediment is another factor that influences the upstream adjustment length. The dimensionless ratio of the adjustment length is independent of the patch density if there is sediment movement on the bed or sediment replenishment far upstream. Due to the difference in composition of the bed surface between the rigid bed and the movable bed, the shear stress is also different, resulting in different changes in the flow velocity around the vegetation patch. Therefore, the upstream adjustment length for the rigid bed is different from that for the movable bed. Moreover, the continuous addition of the sand results in the movable bed being replenished, and the suspended sediment restrains the development of turbulence in the flow; therefore, the region of sediment erosion in the riverbed near the vegetation patch becomes smaller, as reflected by the reduction in upstream adjustment length.

3.2. Wake Region

The centerline velocity of water flowing through the patch wake is defined as the exit velocity, U_e (Figure 2a), which is determined via the depth-averaged velocity at $x/D = 0.8$ due to the limitations of measuring equipment. The region where the depth-averaged velocity of the centerline beyond the end of the vegetation patch decreases sharply for a certain distance and gradually recovers to a steady level is called the "flow wake." The distance from the end edge of the vegetation patch to the point where the depth-averaged velocity of the centerline becomes roughly uniform is defined as the steady wake, and the length of the steady wake is denoted as L_1 (see Figure 2a). Correspondingly, the constant velocity behind the patch is called the steady wake velocity, which is denoted by U_1 (see Figure 2a). The distance whereby the velocity is restored from the uniform value to the point where the growth rate falls below 0.05 is called the wake recovery region, which is denoted as L_2 (see Figure 2a). There is a sudden decline in the depth-averaged velocity within the vegetation patch, resulting in a linear relationship occurring for all patch densities, a finding that is consistent with that of Chen et al. [30]. Therefore, the dimensionless exit velocity U_e/U_0 may be expressed as,

$$\frac{U_e}{U_0} = \frac{U_a}{U_0} - \varepsilon\frac{D}{L} = 1 - \beta\frac{D}{L} \tag{6}$$

The non-dimensional rate of the mean velocity variation may be considered a constant, which is denoted as ε. From the data, ε, which was obtained via a fit using the least squares method to measure the upstream adjusted velocities and exit velocities, is about 0.13 ± 0.03 for all cases. The scale factor β is estimated via the measured velocity, which is about 0.35 ± 0.04 in this experiment. Belcher et al. suggested that the length of the flow adjustment region was impacted by the half width of the patch and the canopy drag length scale [31]. Additionally, Rominger and Nepf employed a finite rectangular emergent

canopy to study the adjustment of flow and proposed that the canopy half-width b and the canopy drag length scale $(C_D a)^{-1}$ are the factors for this adjustment [14]. Hence, one can see that the length of the flow adjustment region may be determined using the width scale of the vegetation patch rather than the shape of the patch. Drawing on their momentum balance equations, we divide by the inertial term in each equation and adopt dual scales for the spatial scale of the adjustment length. This leads to a simplified dependence on the scale of the flow adjustment near the porous circular patch to be obtained:

$$L \sim \left[\left(\frac{\pi d(1-\varphi)}{2C_D\varphi} \right)^2 + \left(\frac{D}{2} \right)^2 \right]^{\frac{1}{2}} \quad (7)$$

where C_D is the drag coefficient, which depends on the solid volume fraction φ and the Reynolds number Re_p.

According to the measured exit velocity, Figure 3a shows a variation in dimensionless U_e with patch density. For the case of a rigid bed, the exit velocity U_e decreases gradually with increasing patch density when $\varphi < 13\%$ ($a < 0.4$ cm^{-1}), then U_e decreases sharply and the deceleration rate is slightly greater when $\varphi \geq 13\%$. The maximum value of U_e is just over $0.7U_0$, and the minimum value is roughly $0.25U_0$. For both the movable bed and the feeding sediment cases, U_e decreases slightly as φ rises, and the difference in U_e between these two cases is not clear. When the patch density is low, the U_e values for the three types of beds are quite distinct. The exit velocity for the rigid bed reaches about $0.7U_0$, which is markedly greater than those in the other two cases, and the U_e values for the other two cases are around $0.5U_0$. The bed elevation dynamically changes for the movable bed and the feeding sediment cases, the sediment erodes, and the corresponding depth of the flow increases, resulting in a reduction in velocity. However, when the patch density is high, there is little difference in U_e for these three cases, and all three velocities are quite similar. The exit velocity is about $0.4U_0$~$0.45U_0$ for both the movable bed and the feeding sediment cases and just under $0.4U_0$ for the rigid bed case. The flow is strongly resisted by a dense vegetation patch, and the sediment and flow around the vegetation are seriously disturbed; therefore, both the bed surface and water surface are dynamic. This dual effect causes no significant variation in U_e for these three-bed conditions. Hence, the interaction between the sediment, the flow, and the vegetation results in a significant variation of the exit velocity.

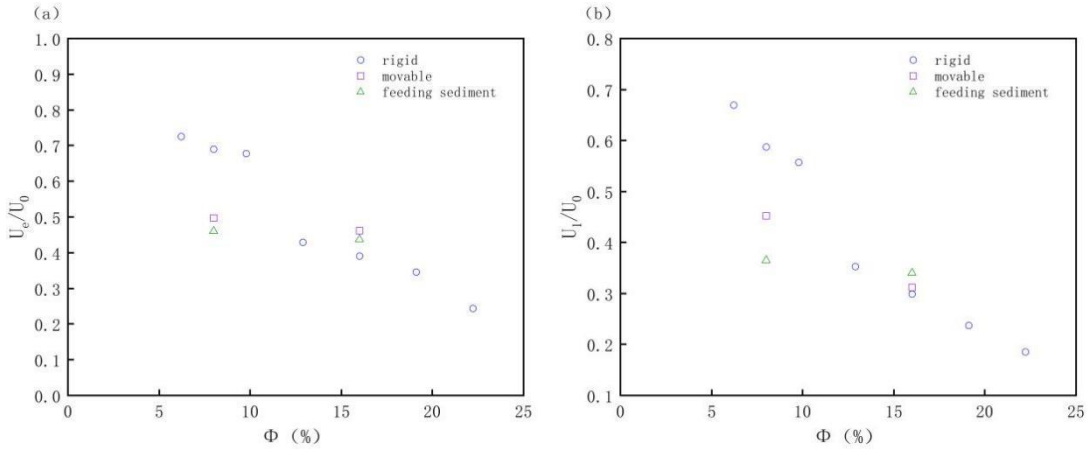

Figure 3. (**a**) Variation in the exit velocity, U_e, with the density of the vegetation patch for all bed conditions. (**b**) Variation in the steady wake velocity, U_1, with the density of the vegetation patch for all bed conditions.

The streamwise velocity behind the wake of the patch keeps decelerating for a distance of L_1 from U_e to U_1. Zong and Nepf suggested that the ratio of the dimensionless velocity

behind the vegetation patch was comparable to or scaled to the dimensionless deceleration through the patch [32]. It may be assumed that U_1 can be written as

$$\frac{U_1}{U_0} = 1 - \mu \frac{D}{L} \tag{8}$$

The fitting of the measured steady wake velocity in this experiment provided the coefficient $\mu = 0.4 \pm 0.03$. It can be clearly seen that U_1 decreases gradually as φ increases, with the maximum occurring at $0.7U_0$ and the minimum reaching $0.2U_0$ for the rigid bed case (Figure 3b). There was a definite downward trend in the variation of U_1 for the movable bed case, whereas the variation of U_1 for the feeding sediment case was indistinct, with a value of $0.35U_0$. At a low density, U_1 was the maximum for the rigid bed case, with values ranging from $0.58U_0$ to $0.7U_0$, while for the movable bed case, the value was the minimum and under $0.4U_0$. When sediment was supplied upstream, U_1 was between the values for the other two cases and was around $0.5U_0$. For high-density, there were subtle differences in the U_1 values in the three cases, and the variation was less than $0.05U_0$. The observations support the fact that both the patch density and the bed form are critical factors in determining the steady wake velocity. In addition, sediment replenishment causes a slight change in the steady wake velocity. As sediment moves in the bed, and even when sediment is supplied upstream of the flume, the exchange between the bed load and the bed material causes increased complexity and variability in the bed morphology. Hence, the interaction between the flow and the vegetation patch is also complex, resulting in many uncertainties in terms of velocity.

The flow is divided into two regions at the cross section where it reaches U_1, causing shear layers on both sides of the steady wake. These layers continue to grow until they intersect at the centerline of the wake. Given that there is an interface between these two shear layers, a Karman vortex street may eventually form. Therefore, the length of the steady wake may be evaluated by considering the development of the shear layers. Drawing on the growth of the shear layer defined by Zong and Nepf, Chen deduced an approximate expression for the shear layer [30,32], which depends on L_1. Based on the observations, the value of L_1 dramatically declines as the patch density increases for the rigid bed and movable bed cases, but the variation in L_1 remains on a plateau with a slow reduction for the feeding sediment case, which then levels off at $3D$ (Figure 4a). For the low patch density, the maximum L_1 cloud exceeds $12D$ for the rigid bed case, but it may not reach this level for the feeding sediment case according to the tendency of the distribution. For both the low-density and high-density cases, L_1 is the largest for the rigid bed case and the smallest for the feeding sediment case. Indeed, there may be suspended sediment in the flow when the sediment is added to the flume, which inhibits the development of the shear layers; therefore, the formation of the steady wake is affected, and the length of the steady wake remains almost unchanged. Moreover, there may be a relationship between L_1 and U_1, which are normalized by D and U_0, respectively. In general, the measured data of the steady wake indicate that L_1/D increases as U_1/U_0 increases (Figure 4b); specifically, when $U_1/U_0 < 0.4$, L_1 tends to be stable. Conversely, the dimensionless length of the steady wake increases more steeply with the increase in steady wake velocity for both the rigid and movable bed cases. Additionally, the variation in L_1/D with U_1/U_0 is relatively insignificant in the feeding sediment case. Therefore, the length of the steady wake depends on the velocity of the steady wake, which is in agreement with the study of Chen [30], where an equation was used to describe the relationship between L_1/D and U_1/U_0.

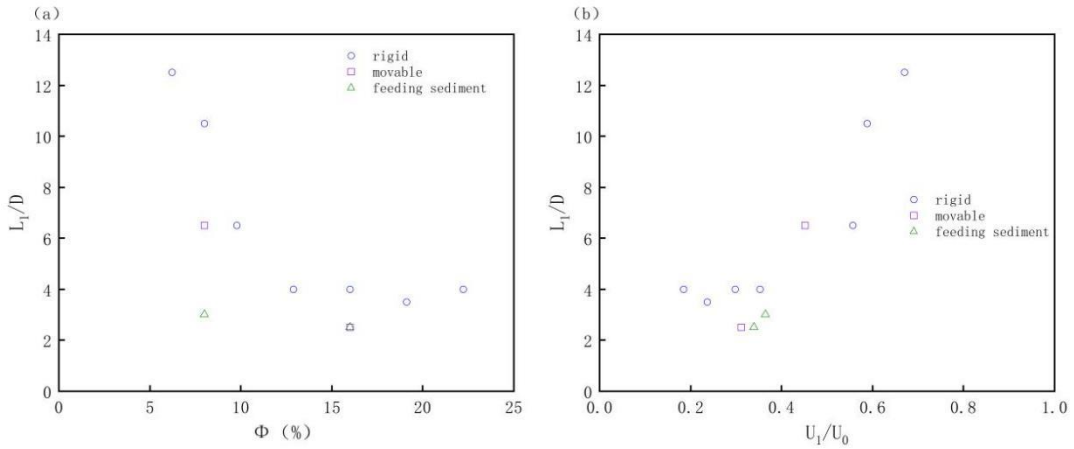

Figure 4. (**a**) Variation in the length of the steady wake, L_1/D, with the density of the vegetation patch for all bed conditions. (**b**) Variation in L_1/D with U_1/U_0 for all bed conditions.

3.3. Reacceleration Region

After the steady wake region, in which the two shear layers develop to the extent that they meet and form the von Karman vortex street, the depth-averaged velocity of the centerline reaccelerates distinctly for a distance L_2 (see Figure 2a). For the normalization of L_2 via D, the measured data show that L_2/D fluctuates with φ (Figure 5a) for all three bed conditions. More specifically, for the rigid bed case, there is an upward trend in L_2 when the patch density is low, with values ranging from $8D$ to $14D$. There is a clear decrease in L_2 when φ is less than 13%, and thus the length of the wake recovery is around $11D$ when the patch density is high. For the movable bed and the feeding sediment cases, the L_2 for the low-density case is less than that for the high-density case, and the L_2 for the former is greater than that for the latter when the patch density is the same. Meanwhile, the difference in values between the low-density and high-density cases is greater for these two bed conditions. When the patch density is low ($a < 0.4$ cm^{-1}), the more porous the vegetation patch is, the closer together both the reacceleration regions and the velocity recovery are located downstream. For the high-density patches ($a \geq 0.4$ cm^{-1}), the velocity of the flow behind the patch wake rapidly reaccelerates for a short distance when the porosity of the vegetation patch is smaller. However, the gaps between locations of reacceleration for the different patch densities and the distances between positions of the restored velocities are not the same. Additionally, when the bed is movable or sediment is supplied upstream, the velocity may rise prematurely compared with that for the rigid bed case. Evidently, positions where the velocity begins to rise and where it resumes can be used to determine L_2, which is affected by both the bed form and the patch density. Since L_2 is determined using the cross-section where the velocity starts to increase, there should be a dependence between U_1 and L_2. As expected, the variation in L_2/D with U_1/U_0 for the different bedforms is shown in Figure 5b. For the rigid bed case, L_2/D remains at 11 when $U_1/U_0 < 0.4$, and then it moves upwards and finally decreases as U_1/U_0 increases, resulting in an overall downward trend in development. Moreover, L_2/D decreases as U_1/U_0 increases for the movable bed and the feeding sediment cases, with a more dramatic variation in the latter. This phenomenon occurs due to the significant rate of change in velocity in these situations. In the steady wake, there is a constant velocity of U_1 and the flow outside this region is also uniform, denoted as U_{os}. We define the velocity difference as ΔU, i.e., $\Delta U = U_{os} - U_1$, which determines the growth rate of the shear layer. The development of the shear layer is closely related to the formation of the von Karman vortex street, which is an important indicator of the steady wake decay. Thus, there is evidence supporting the idea of a potential relationship between L_2 and ΔU. Although the bedforms are different, L_2/D drastically increases with the increase in $\Delta U/U_0$ when $\Delta U/U_0 < 0.5$, especially for the feeding sediment case (Figure 5c). However, $\Delta U/U_0 \geq 0.6$, L_2/D hardly changes as $\Delta U/U_0$ increases.

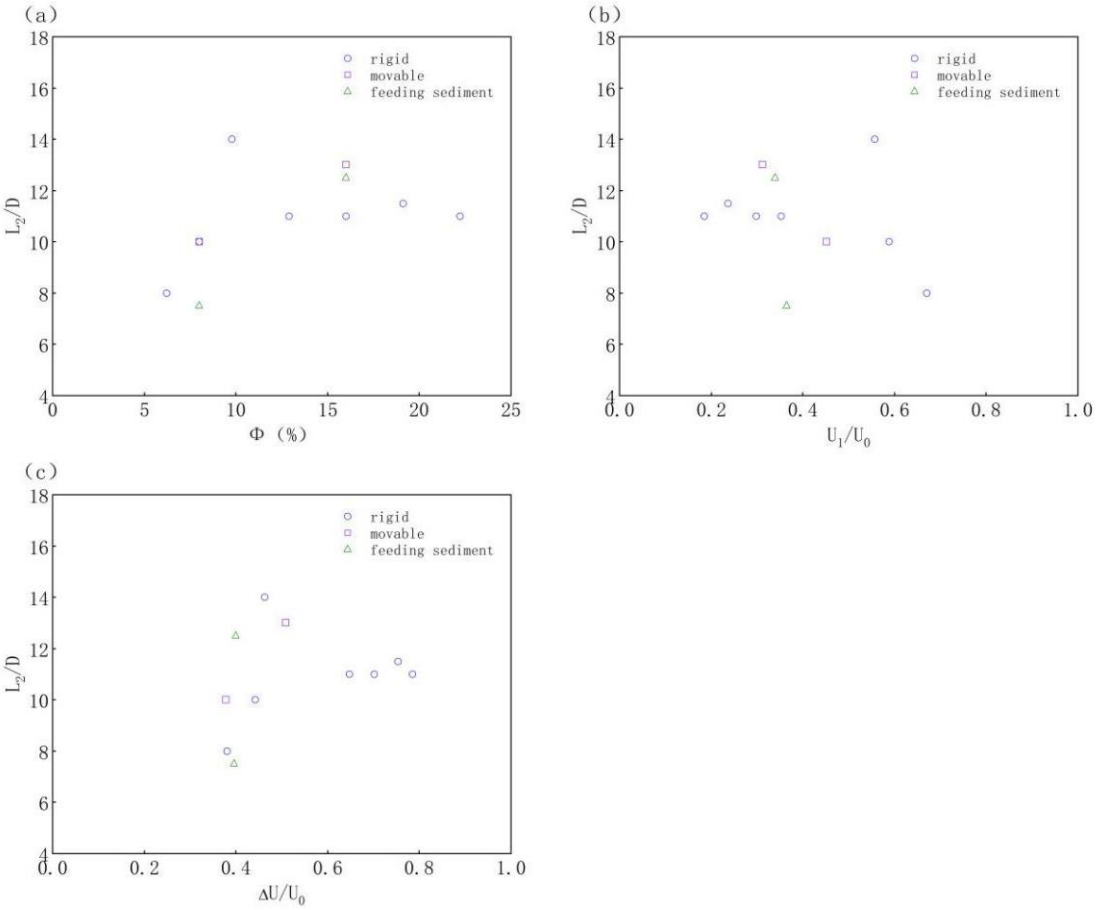

Figure 5. Variation in L_2/D with, φ, U_1/U_0 and $\triangle U/U_0$ for all bed conditions. (**a**) Variation in the dimensionless length of the wake recovery, L_2/D, with the solid volume fraction. (**b**) The relation between the dimensionless length of the wake recovery region, L_2/D, and the velocity ratio U_1/U_0. (**c**) The relation between the dimensionless length of the wake recovery region, L_2/D, and the velocity ratio $\Delta U/U_0$.

3.4. Altimetric Topographic Maps for the Different Densities and Bed Conditions

Bed morphology changes as a result of sediment transport, causing the formation of various beds. This study examines the bed morphodynamics for the movable and feeding sediment bed conditions, with patch densities of 0.25 cm^{-1} and 0.5 cm^{-1}. The experiment continued for three days to ensure the full development of the bed. The formation of the bed was monitored using an electronic total station and a digital camera, and the data were then transformed via three-dimensional modeling technology to generate the altimetric topographic maps and simplified planar effect drawings shown in Figures 4 and 5, respectively. Figure 6 shows that the bed surface behind the vegetation patch is not flat because of the interaction between the flow, the vegetation, and the sediment. Behind the wake of the patch, the sediment is uplifted, forming a hillock that develops into a narrow strip before disappearing. Eventually, the bed surface becomes flat. Scour holes are formed on both sides of the vegetation patch, and their depths increase as the density of vegetation increases. A comparison of the results shown in Figures 4c and 6b demonstrates that the incoming sediment causes minor changes to the bed surface. As a result, the hillock becomes wider, the scour holes on both sides of the patch become shallower, and the narrow strip grows longer.

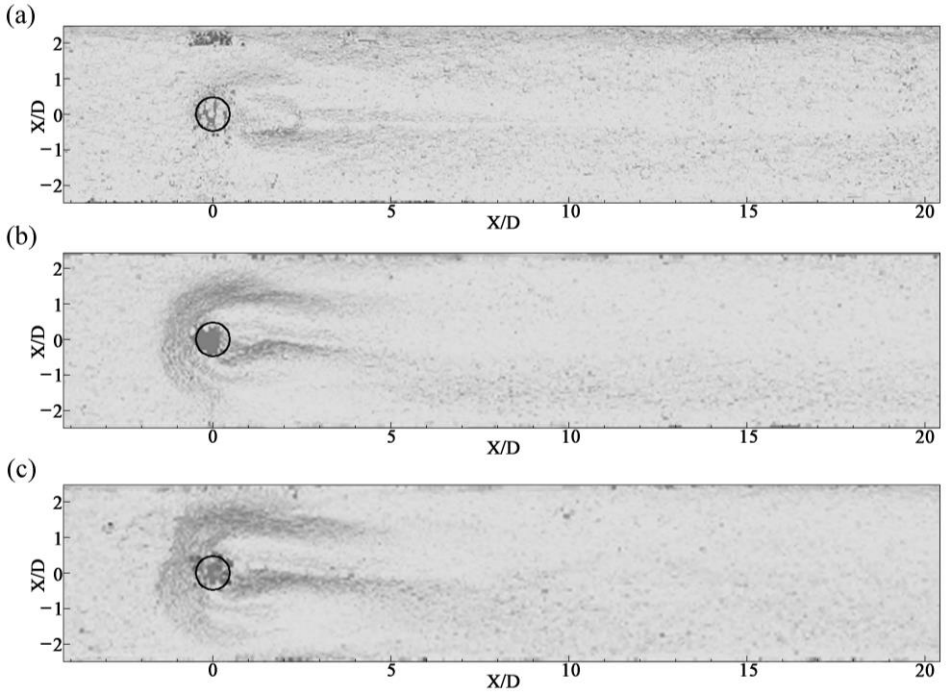

Figure 6. Simplified drawing of the planar effect for different cases. The black circle represents the location of the model patch. (**a**) The density is 0.25 cm^{-1}, and the bed condition is movable (Case Anm1). (**b**) The density is 0.5 cm^{-1}, and the bed condition is movable (Case Anm2). (**c**) The density is 0.5 cm^{-1}, and the condition is feeding sediment (Case Anf2).

The bed elevation is reflected in the altimetric topographic map shown in Figure 7, illustrating that the bed elevation around the patch is relatively low. In particular, the elevation of the centerline behind the patch wake is relatively higher than that of both sides of the centerline, which is consistent with the simplified planar effect of the drawing (Figure 6). Evidently, there are two symmetrical "sand tails" behind the patch (Figure 7). Combined with the color bar, it may be observed that, even though there is a small hillock behind the patch, the bed remains eroded and the elevation decreases in all cases, with varying degrees of decline. As stated earlier, the decrease in the erosion rate is mainly caused by the patch resistance to the flow, causing a reduction in bed erosion. Although the vegetation patch can impede the sediment movement within it, the sediment in the surrounding areas is disturbed as a result of the resistance of the vegetation to the flow. This aggravates the sediment movement and ultimately results in the erosion of the sediment in the vicinity of the vegetation.

Moreover, the bed elevation of the sour holes on both sides around the patch is greater when the vegetation is dense compared to when it is sparse ($a < 0.4$ cm^{-1}, Figures 5b and 7a), but the length of the sour holes is smaller for dense vegetation ($a > 0.4$ cm^{-1}) than that for sparse vegetation. Additionally, the elevation of the hillock in the wake of the patch is greater in the dense case compared to the sparse case. The length of the narrow strip of sediment behind the patch decreases as the patch density increases. Tseng and Tinoco and Yang et al. indicated that although vegetation can exert resistance and slow down the flow, it can also generate turbulence that enhances sediment transport [25,26]. However, when the vegetation patch is dense, the turbulence effect is limited. With the increase in patch density, the resistance of the vegetation patch to the flow increases; therefore, the flow velocity decreases, resulting in a decrease in sediment carrying capacity. Consequently, the rate of sediment transport slows down, causing the corresponding elevation to increase and the area of the riverbed affected by vegetation to be reduced. Comparing Figures 7b and 8c, it may be observed that the bed elevation is greater in the case of sediment supply, and the incoming sediment is attributed to the longer "sand tail" in the region.

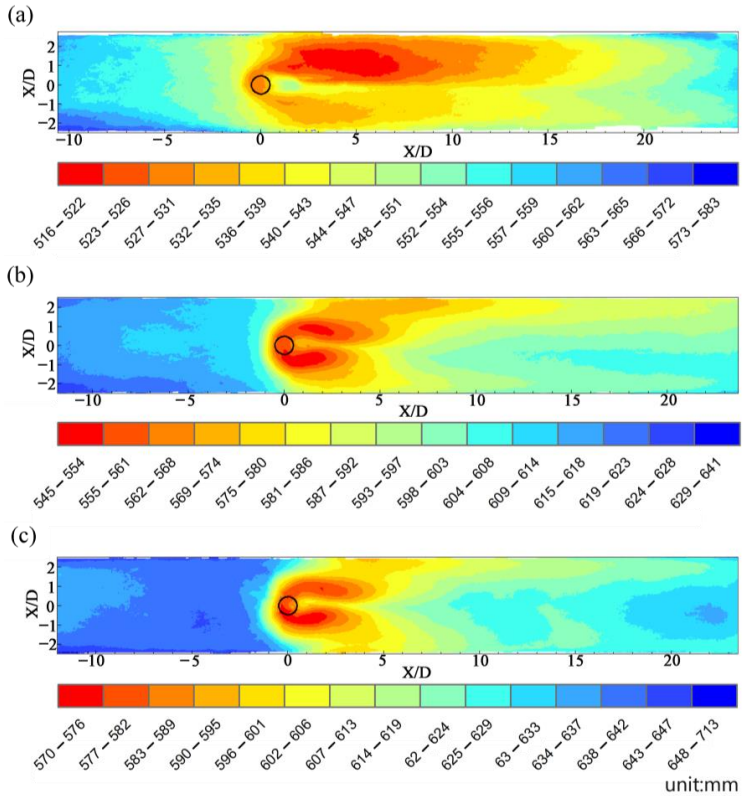

Figure 7. Altimetric topographic maps for different cases. The unit of the bed elevation is mm in all cases. The black circle represents the location of the model patch. (**a**) The density is 0.25 cm^{-1}, and the bed condition is movable (Case Anm1). (**b**) The density is 0.5 cm^{-1}, and the bed condition is movable (Case Anm2). (**c**) The density is 0.5 cm^{-1}, and the condition is feeding sediment (Case Anf2). The altimetric topographic map can reflect the specific elevation in all of the region. The color bar indicates the varied elevation around the bed surface.

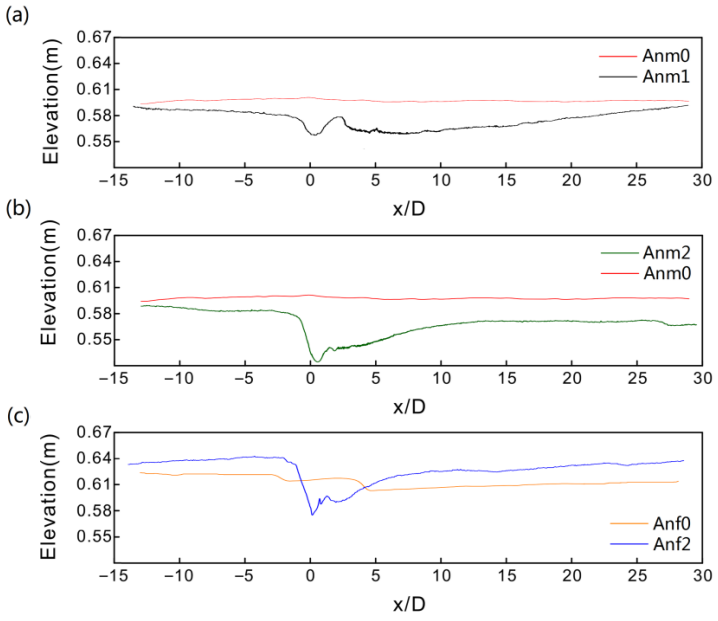

Figure 8. The longitudinal distribution of bed elevation along the channel centerline for different cases. (**a**) The density is 0.25 cm^{-1}, and the bed condition is movable (Case Anm1). (**b**) The density is 0.5 cm^{-1}, and the bed condition is movable (Case Anm2). (**c**) The density is 0.5 cm^{-1}, and the condition is feeding sediment (Case Anf2). The red and orange lines represent the non-vegetation case. The figures directly reflect changes in the scouring and silting of the bed.

3.5. Longitudinal Distribution of the Bed Elevation Along the Central Line

The altimetric topographic maps above show a significant change in bed morphology along the central line in the lee of the patch, primarily due to sediment transport. For a detailed investigation of bed deformation, we selected the elevation along the central line ($y/D = 0$) based on a three-dimensional plot of various bed forms generated by software, as shown in Figure 8. This figure illustrates that the morphodynamics of the downstream bed were significantly affected by the vegetation patch and the incoming upstream sediment. Compared to the non-vegetated case, it is evident that the elevation of the bed decreased, most likely due to the presence of the vegetation patch that intercepted some sediment. The interception of sediment by the vegetation patch immediately lowers the bed surface in the lee of the patch. The bed surface then gradually rises downstream due to the longitudinal deposition of the sediment. More sediment deposition occurs if sediment is supplied upstream of the flume under the experimental conditions.

4. Discussion

4.1. Relationship between Bed Morphology and Flow Structure

The presence of vegetation not only affects the flow field but also causes a change in the turbulence field. Turbulence has significant effects on sediment transport and bank erosion. Additionally, the turbulence can cause an increase in the sediment-carrying capacity of the flow, thereby increasing sediment transport. Graf and Istiarto found that sediment erosion and the associated transfer intensity increased with an increase in turbulence intensity [33]. Both Tseng and Tinoco and Yang et al. have already addressed the fact that the near-bed value of TKE is the key factor driving sediment motion in vegetated flows [25,26]. This increase in this value is caused by both bed shear and vegetation stems. Therefore, the depth-averaged value can be used to underestimate the real effect of turbulence on sediment motion. However, in such a dense vegetation patch ($a > 0.25$), vegetation-generated turbulence is dominant, and the bed-shear component can be ignored.

At the leading edge of the patch, the depth-average velocity gradually decreases, and the bed elevation also decreases. The distance from the section where the bed elevation starts to decline to the first trough position behind the patch is defined as the transitional length L_{e0}, and the corresponding minimum elevation is denoted as E_0 (see Figure 9). At the patch wake, because of the water-blocking effect of the vegetation patch, the velocity through the patch decelerates and the TKE rises (Figure 10). Correspondingly, the sediment movement is enhanced, which is reflected in a decrease in bed elevation. This dramatic change in the flow structure is related to the turbulence generated by the cylinder with the patch [31]. Therefore, the reduction in bed elevation is not permanent, and the momentum of the river current is sufficient to enhance the sediment movement, causing an increase in bed elevation. After a short distance, the elevation reaches its maximum value. The distance from the minimum behind the patch to this position is defined as the rising length L_{e1}, and the elevation of this position is denoted as E_1. At this location, the TKE reaches a minimum, where the flow is not affected by the shear layer and the velocity is the main factor of the TKE [30]. The flow turbulence is restricted in this area due to its low velocity, and sediment movement slows down, which causes an increase in bed elevation. However, the flow is then affected by the shear layer, resulting in the generation of a vortex [14]. There is a strong exchange of momentum, and thus the intensity of the turbulence rapidly increases, which enhances the movement of the sediment and leads to a sudden drop in bed elevation. The bed elevation then gradually decreases and reaches a minimum for the second time. The distance from the peak position to the second trough position is defined as the adjustment length L_{e2}, and the corresponding elevation is denoted as E_2 (see Figure 9). The location of E_2 is almost the same as that of U_1. Both the velocity and TKE then increase, as does the bed elevation. It is at this point that the steady wake begins to decay. The recovery of the elevation is related to the formation of the vortex street. Affected by the large-scale oscillation of the wake, the second peak of the TKE occurs farther downstream, and then the TKE decays. Meanwhile, the velocity continues to increase, and the bed

morphology becomes steady. Therefore, the evolution of bed morphology is closely linked to the TKE and the growth of the vortex street. Behind the wake of the patch, in a process where the TKE decreases from the first peak, the bed elevation gradually increases when the variation in TKE becomes relatively small, and the sediment is most deposited when the TKE reaches the minimum value. At the center of the von Karman vortex street, the TKE arrives at the second peak, and the bed elevation recovers to approximately the same level as that far upstream.

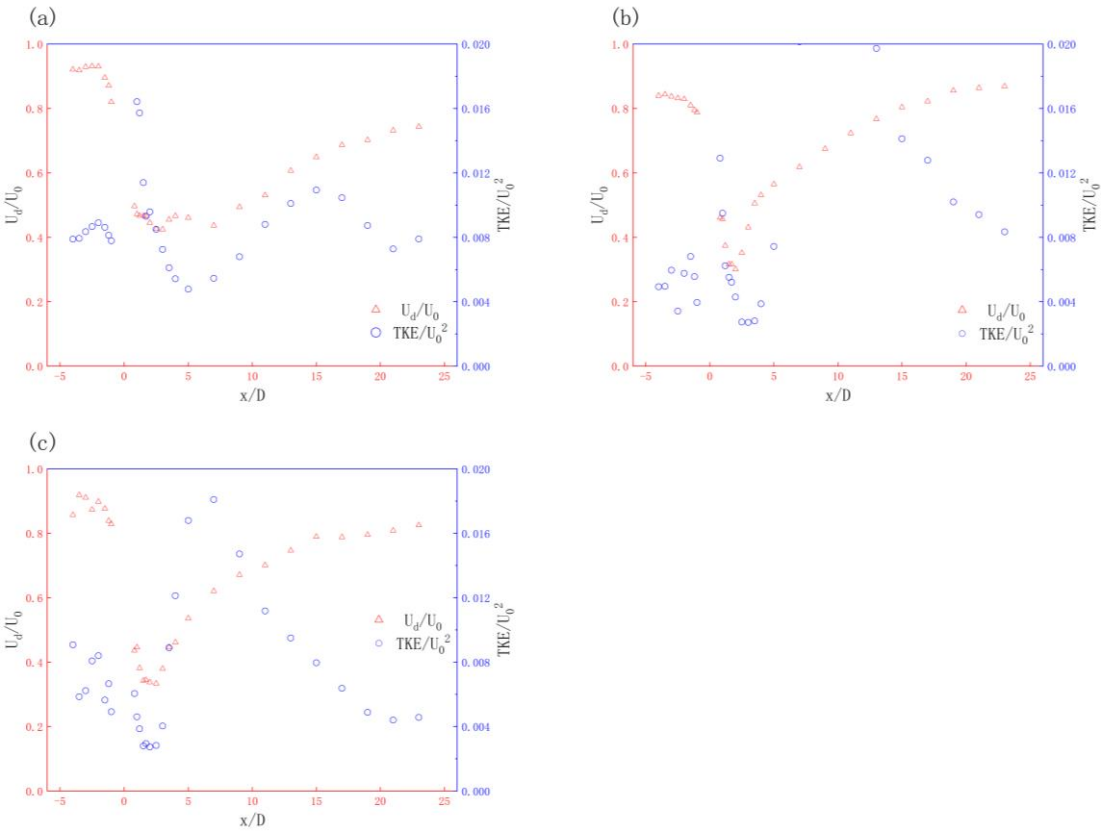

Figure 9. The longitudinal distributions of bed elevation along the channel centerline for different cases. (**a**) The density is 0.25 cm^{-1}, and the bed condition is movable (Case Anm1). (**b**) The density is 0.5 cm^{-1}, and the bed condition is movable (Case Anm2). (**c**) The density is 0.5 cm^{-1}, and the condition is feeding sediment (Case Anf2).

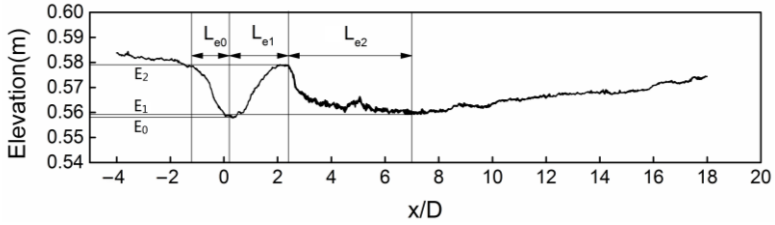

Figure 10. Schematic of the transitional length, the rising length, and the adjusted length. L_{e0} is the transitional length, L_{e1} is the rising length, and L_{e2} is the adjusted length. The density is 0.25 cm^{-1}, and the bed condition is movable (Case Anm1).

4.2. The Effects of Vegetation Density and Feeding Sediment on Bed Morphology

In the previous discussion, both the patch density and the bed form were found to be crucial factors in determining the flow velocity and TKE. Additionally, the variation in bed elevation was determined by the development of the TKE. Therefore, it can be concluded that there may be a correlation between the variables. The fact that L_{e0}, L_{e1}, and L_{e2}

distinctly vary in these cases is supported by a comparison of the longitudinal distribution of bed elevation along the channel centerline with different patch densities and incoming sediment (Figure 11). At a position upstream of the leading edge of the patch, the bed elevation decreases sharply, and this downward trend follows an almost linear pattern in all cases. When sediment is supplied upstream, the elevation first reaches the bottom of the bed just behind the patch wake, and the measured data indicate that L_{e0} is approximately $1.5D$ for the dense case. For the same patch density, the elevation continues to decrease for a short distance behind the patch wake, and $L_{e0} = 2D$ with no incoming sediment. When the patch is sparse, $L_{e0} = 1.5D$. In these three cases, the vegetation patch has less of an effect on the bed upstream, and the impact region remains within the patch's diameter. There is little difference in the value of L_{e0} between the sparse and dense cases. There may be disturbance as the water flows through the vegetation patch and sediment transport enhances, resulting in bed erosion. The impact area is determined by cylinders within the vegetation patch at a stem-scale level. Therefore, the change in L_{e0} is not sensitive to patch density or incoming sediment. In all cases, E_0 is located nearly at the patch wake, where the TKE reaches the first peak. The turbulence is generated by the shear stress of the flow and the resistance of the vegetation, and the TKE increases suddenly, resulting in a reduction in bed elevation. As the patch density increases, the first maximum value of the TKE decreases, sediment transport enhances, and thus the bed elevation decreases. The value of E_0 for these three cases is less than the original bed elevation, so the bed is eroded at this position. The elevation far upstream is denoted by E_∞, and the difference in elevation for the transitional length, L_{e0}, is denoted as $\Delta E_0 = E_\infty - E_0$. From the observations, it can be found that ΔE_0 is nearly identical for both the feeding sediment case and the movable bed case. The incoming sediment may have a negligible impact on the difference in elevation between the far upstream and the patch wake. For the same bed form and flow condition, ΔE_0 increases with the patch density. As vegetation density increases, patch resistance to the flow also increases. This in turn results in enhanced erosion of the bed, leading to a greater reduction in bed elevation.

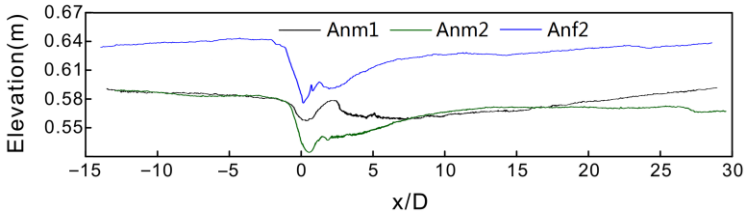

Figure 11. The longitudinal distribution of bed elevation along the channel centerline for Case Anm1, Case Anm2, and Case Anf2.

For the first maximum elevation in the upward trend behind the patch, the difference between its maximum and minimum values is defined as ΔE_1, i.e., $\Delta E_1 = E_1 - E_0$. The value of L_{e1} decreases as the density of the patch increases, and the position of E_1 moves upstream with increased patch density. For the same patch density, L_{e1} remains almost constant at $1D$, and the variation in L_{e1} is not very clear when the sediment is supplied upstream (Figure 11). For the same bed condition, L_{e1} is approximately $2D$, and with the increase in patch density, the velocity reaches the low-velocity area earlier, causing sediment deposition and a decline in L_{e1} to occur earlier. However, this variation may not occur when sediment is supplied upstream of the flume. Both E_1 and ΔE_1 decrease with increasing patch density and increase when the sediment is supplied upstream. Actually, although the elevation is at a maximum, the bed is still in a state of scouring in all cases when compared to its original elevation. Clearly, the amount of incoming sediment supplied upstream is not sufficient to sustain sediment deposition. It is the patch density that dominates the bed elevation behind the patch.

Next, there is the second downward trend in bed elevation behind the patch, and the difference in elevation between the maximum and the second minimum is denoted as

ΔE_2, i.e., $\Delta E_2 = E_1 - E_2$. For high patch density, the values of L_{e2} for the feeding sediment and movable bed cases are 1.2D and 0.5D, respectively (Figure 11), which means that the position of E_2 moves slightly downstream with the incoming sediment. Compared to the high-density condition, L_{e2} is significantly larger for a low patch density, which is almost 6.5 D. The location of E_2 is further downstream, illustrating that L_{e2} decreases with increasing patch density. Since the position of E_2 is related to the length of the steady wake, L_1, which decreases as the patch density increases, L_{e2} also decreases. Both E_2 and ΔE_2 decrease as the patch density increases. When sediment is added, E_2 significantly increases, yet ΔE_2 remains unchanged. Finally, there is a recovery process for bed elevation, where elevation rises gradually far upstream. The bed elevation rapidly recovers when the patch density is high, meaning that the length of the recovery decreases as the patch density increases. Additionally, if the sediment is replenished upstream, the rate of recovery is faster and the recovery process is shorter. A von Karman vortex street is formed from the interactions between the shear layers after the steady wake [34]. At the center of the von Karman vortex street, the TKE reaches its second maximum value, leading to the gradual deposition of sediment.

5. Conclusions

In this study, systematic laboratory experiments were conducted to investigate velocity, TKE distribution, and bed morphology in a patch-vegetated flume with and without incoming sediment. The following key findings are based on the experimental results:

(1) The upstream adjustment velocity U_a remains almost constant at a low density, but it slightly decreases as the volume fraction increases when the patch density is high. The movable bed form contributes to a reduction in U_a, while the incoming sediment causes an increase. The length of the upstream adjustment region (L_0) is greater in the high-density condition. However, the value remains nearly constant, whether the patch is sparse or dense.

(2) Both the exit velocity U_e and the steady wake velocity U_1 gradually decrease with the increasing solid volume fraction φ. They also decrease with the sediment supply when the patch density is low but show little change under high-density conditions.

(3) The length of the recovery region L_2 increases with the density when the patch is sparse, and it remains constant for the dense patch. The incoming sediment causes a reduction in L_2, decreasing as U_1/U_0 increases.

(4) Turbulent kinetic energy varies depending on the bed form. The value of the first peak is greater than that of the second peak in all bed conditions. The incoming sediment causes a decrease in the magnitude of the difference between these two peaks. Because of the sediment, the position of the second peak is closer to the patch, and this value is greater.

(5) The depth of the scour holes on both sides of the patch increases as the vegetation density increases. The incoming sediment leads to the hillocks becoming wider, the scour holes becoming shallower, and the narrow strip becoming longer. Significantly, the development of bed morphology is closely related to the TKE and the increase in the vortex street.

Based on the concept of landscape hydrology, river restoration may achieve the goal of restoring the ecological function of a river by designing and arranging its landscape, such as various vegetation patches. It is crucial to comprehend the relationship between river evolution and various driving factors [35]. The results enhance our understanding of how different densities of vegetation patches affect the erosion and deposition of sediment in a riverbed and the potential mechanisms of incoming suspended sediment around the vegetation patch. It is helpful for the appropriate density of the landscape vegetation to be determined based on the water and sediment conditions of the river. This arrangement may beautify and restore water channels. Significantly, it may provide a scientific basis for the ecological restoration of rivers and natural channel construction.

There are some limitations to this study. For example, this study involves a few experiments in the condition of feeding-sediment, and there is no change in the supplement gradient throughout the experiments. Therefore, the results can only demonstrate the comparison of changes in flow structure and bed morphology with and without sediment supply. Due to limitations, only qualitative analyses were made without quantitative calculations. In future research, I plan to design experiments with varying quantities of sediment supply to further investigate the effects of the amount and speed of incoming sediment on the flow structure and bedform. Qualitative analysis and calculations should be conducted to establish relevant models.

Author Contributions: Conceptualization, D.W.; methodology, D.W.; investigation, D.W.; data curation, D.W.; writing—original draft preparation, D.W. and F.L.; writing—review and editing, D.W.; supervision, K.Y. All authors have read and agreed to the published version of the manuscript.

Funding: This study was financially supported by the National Key Research and Development Program of China (Grant No. 2022YFE0128200) and the National Natural Science Foundation of China (Grant No. 51979181).

Data Availability Statement: The data presented in this study are available on request from the corresponding author. The data are not publicly available as the author's series of experiments are not yet complete.

Acknowledgments: The authors are very grateful to Yakun Guo for his suggestions on manuscript revision.

Conflicts of Interest: The authors declare no conflict of interest.

References

1. Moradi Larmaei, M.; Mahdi, T.F. Depth-averaged turbulent heat and fluid flow in a vegetated porous medium. *Int. J. Heat Mass Transf.* **2012**, *55*, 848–863. [CrossRef]
2. Nepf, H.M.; Sullivan, J.A.; Zavistoski, R.A. A model for dif- fusion within emergent vegetation. *Am. Soc. Limnol. Oceanogr.* **1997**, *42*, 1735–1745. [CrossRef]
3. Horritt, M.S. A linearized approach to flow resistance uncertainty in a 2-D finite volume model of flood flow. *J. Hydrol.* **2006**, *316*, 13–27. [CrossRef]
4. Zhang, J.T.; Su, X.H. Numerical model for flow motion with vegetation. *J. Hydrodyn.* **2008**, *20*, 172–178. [CrossRef]
5. Zhang, H.; Dai, L. Surface runoff and its erosion energy in a partially continuous system: An Ecological Hydraulic Model. In Proceedings of the 2010 ASME International Mechanical Engineering Congress and Exposition, Lake Buena Vista, FL, USA, 13–19 November 2009; Volume 10, pp. 575–583.
6. Wang, P.F.; Wang, C. Numerical model for flow through submerged vegetation regions in a shallow lake. *J. Hydrodyn.* **2011**, *23*, 170–178. [CrossRef]
7. Wilson, C.A.M.E.; Stoesser, T.; Bates, P.D.; Bateman Pinzen, A. Open channel flow through different forms of submerged flexible vegetation. *J. Hydraul. Eng.* **2003**, *129*, 847–853. [CrossRef]
8. Tal, M.; Paola, C. Dynamic single-thread channels maintained by the interaction of flow and vegetation. *Geology* **2007**, *35*, 1651–1656. [CrossRef]
9. Braudrick, C.A.; Dietrich, W.E.; Leverich, G.T.; Sklar, L.S. Experimental evidence for the conditions necessary to sustain meandering in coarse-bedded rivers. *Proc. Natl. Acad. Sci. USA* **2009**, *106*, 16936–16941. [CrossRef]
10. Cotton, J.A.; Wharton, G.; Bass, J.; Heppell, C.M.; Wotton, R.S. The effects of seasonal changes to in-stream vegetation cover on patterns of flow and accumulation of sediment. *Geomorphology* **2006**, *77*, 320–334. [CrossRef]
11. Gurnell, A.M.; van Oosterhout, M.P.; de Vlieger, B.; Goodson, J.M. Reach-scale interactions between aquatic plants and physical habitat: River Frome, Dorset. *River Res. Appl.* **2006**, *22*, 667–680. [CrossRef]
12. Bennett, S.J.; Wu, W.; Alonso, C.V.; Wang, S.S.Y. Modeling fluvial response to in-stream woody vegetation: Implications for stream corridor restoration. *Earth Surf. Process. Landf.* **2008**, *33*, 890–909. [CrossRef]
13. Bouma, T.J.; Duren, L.; Temmerman, S.; Claverie, T.; Blanco-Garcia, A.; Ysebaert, T.; Herman, P.M.J. Spatial flow and sedimentation patterns within patches of epibenthic structures: Combining field, flume and modelling experiments. *Cont. Shelf Res.* **2007**, *27*, 1020–1045. [CrossRef]
14. Rominger, J.T.; Nepf, H.M. Flow adjustment and interior flow associated with a rectangular porous obstruction. *J. Fluid Mech.* **2011**, *680*, 636–659. [CrossRef]
15. Sukhodolova, T.A.; Sukhodolov, A.N. Vegetated mixing layer around a finite-size patch of submerged plants: 1. Theory and field experiments. *Water Resour. Res.* **2012**, *48*, 268–282. [CrossRef]
16. Olson; Gerland, W. Book Reviews: Biotechnical slope protection and erosion control. *Soil Sci.* **1982**, *135*, 126. [CrossRef]

17. Temmerman, S.; Bouma, T.J.; Van de Koppel, J.; Van der Wal, D.; De Vries, M.B.; Heman, P.M.J. Vegetation causes channel erosion in a tidal landscape. *Geology* **2007**, *35*, 631–634. [CrossRef]
18. Liu, C.; Shan, Y.Q. Impact of an emergent model vegetation patch on flow adjustment and velocity. *Proc. Inst. Civ. Eng.-Water Manag.* **2022**, *175*, 55–66. [CrossRef]
19. Liu, C.; Yan, C.H.; Sun, S.C.; Lei, J.R.; Nepf, H.M.; Shan, Y.Q. Velocity, turbulence, and sediment deposition in a channel partially filled with a Phragmites australis canopy. *Water Resour. Res.* **2022**, *58*, e2022WR032381. [CrossRef]
20. Follett, E.M.; Nepf, H.M. Sediment patterns near a model patch of reedy emergent vegetation. *Geomorphology* **2012**, *179*, 141–151. [CrossRef]
21. Chen, Z.; Jiang, C.; Nepf, H.M. Flow adjustment at the leading edge of a submerged aquatic canopy. *Water Resour. Res.* **2013**, *49*, 5537–5551. [CrossRef]
22. Ortiz, A.C.; Ashton, A.; Nepf, H.M. Mean and turbulent velocity fields near rigid and flexible plants and the implications for deposition. *J. Geophys. Res. Earth Surf.* **2013**, *118*, 2585–2599. [CrossRef]
23. Liu, C.; Nepf, H.M. Sediment deposition within and around a finite patch of model vegetation over a range of channel velocity. *Water Resour. Res.* **2016**, *52*, 600–612. [CrossRef]
24. Tinoco, R.O.; Coco, G. A laboratory study on sediment resuspension within arrays of rigid cylinders. *Adv. Water Resour.* **2016**, *92*, 1–9. [CrossRef]
25. Tseng, C.Y.; Tinoco, R.O. A two-layer turbulence-based model to predict suspended sediment concentration in flows with aquatic vegetation. *Geophys. Res. Lett.* **2021**, *48*, e2020GL091255. [CrossRef]
26. Yang, J.Q.; Chung, H.; Nepf, H.M. The onset of sediment transport in vegetated channels predicted by turbulent kinetic energy. *Geophys. Res. Lett.* **2016**, *43*, 11–261. [CrossRef]
27. Furukawa, K.; Wolanski, E.; Mueller, H. Currents and sediment transport in mangrove forests. *Estuar. Coast. Shelf Sci.* **1997**, *44*, 301–310. [CrossRef]
28. Li, W.Q.; Dan, W.; Jiao, J.L.; Yang, K.J. Effects of vegetation patch density on flow velocity characteristics in an open channel. *J. Hydrodyn.* **2018**, *31*, 1052–1059. [CrossRef]
29. Ren, B.L.; Wang, D.; Li, W.Q.; Yang, K. The velocity patterns in rigid and mobile channels with vegetation patches. *J. Hydrodyn.* **2019**, *32*, 561–569. [CrossRef]
30. Chen, Z.; Ortiz, A.; Zong, L.; Nepf, H.M. The wake structure behind a porous obstruction and its implications for deposition near a finite patch of emergent vegetation. *Water Resour. Res.* **2012**, *48*, W09517. [CrossRef]
31. Belcher, S.E.; Jerram, N.; Hunt, J.C.R. Adjustment of a turbulent boundary layer to a canopy of roughness elements. *Fluid Mech.* **2003**, *488*, 369–398. [CrossRef]
32. Zong, L.; Nepf, H.M. Vortex development behind a finite porous obstruction in a channel. *J. Fluid Mech.* **2012**, *691*, 368–391. [CrossRef]
33. Graf, W.H.; Istiarto, I. Flow pattern in the scour hole around a cylinder. *J. Hydraul. Res.* **2002**, *40*, 13–20. [CrossRef]
34. Zong, L.; Nepf, H.M. Flow and deposition in and around a finite patch of vegetation. *Geomorphology* **2010**, *116*, 363–372. [CrossRef]
35. Roni, P.; Liermann, M.; Muhar, S.; Schmutz, S. *Stream and Watershed Restoration: A Guide to Restoring Riverine Processes and Habitats*; Wiley & Sons: Hoboken, NJ, USA, 2012; pp. 254–279.